Stripe Discommensuration and Spin Dynamics of Half-Doped $Pr_{3/2}Sr_{1/2}NiO_4$

Avishek Maity,[1,2,*] Rajesh Dutta,[3,4,†] and Werner Paulus[5]
[1]Institut für Physikalische Chemie, Georg-August-Universität Göttingen, 37077 Göttingen, Germany
[2]Heinz Maier-Leibnitz Zentrum (MLZ), Technische Universität München, 85747 Garching, Germany
[3]Institut für Kristallographie, RWTH Aachen Universität, 52066 Aachen, Germany
[4]Jülich Centre for Neutron Science (JCNS) at Heinz Maier-Leibnitz Zentrum (MLZ), 85747 Garching, Germany
[5]Institut Charles Gerhardt Montpellier, Université de Montpellier, 34095 Montpellier, France

(Received 14 June 2019; revised manuscript received 15 February 2020; accepted 12 March 2020; published 8 April 2020)

We present inelastic neutron scattering measurements of magnetic excitations in stripe ordered $Pr_{3/2}Sr_{1/2}NiO_4$ at $T \sim 10$ K. For the observed magnetic incommensurability $\epsilon = 0.4$, we have incorporated a stripe discommensuration model in our linear spin wave calculation and obtained best agreement with the measured spin wave dispersion, especially to explain the symmetrical outward shift of the magnetic peaks from Néel ordered zone center in energy range 35 to 45 meV. Our study indicates the prerequisite to consider a discommensurated spin stripe unit with proper out-of-plane and in-plane exchange interactions in between Ni^{2+} spins to describe the observed spin wave characteristics in $Pr_{3/2}Sr_{1/2}NiO_4$.

DOI: 10.1103/PhysRevLett.124.147202

Dynamics of charge and spin stripes in strongly correlated 214-type nickelates ($Ln_{2-x}Sr_xNiO_{4+\delta}$) [1–7] have been investigated intensively in the last two decades to understand the possible role of the dynamical stripe correlations to the high-T_c superconductivity observed in the isostructural cuprates [8–12]. The fluctuating stripes in cuprates exist almost in a liquidlike state. In contrast, the stripes in nickelates are pronounced and localized over a wide range of hole doping concentrations $n_h = x + 2\delta$ [13–15]. Studies on spatially inhomogeneous charge and spin stripe correlations, aiming to uncover the importance of spin fluctuation mediated high-T_c superconductivity are, however, not only limited to cuprates but involve increasingly the isostructural insulating nickelates and cobaltates. Comprehensive studies on magnetic excitations in $La_{2-x}Sr_xNiO_4$ ($0.275 \leq x \leq 0.5$) have given further insight on the inter- and intrastripes spin-spin correlations and the observed spin wave dispersions have been interpreted by linear spin wave (LSW) calculation, taking into account the commensurate stripes only [2,4–6].

In the half-doped $La_{3/2}Sr_{1/2}NiO_4$ with $\epsilon \approx 0.44$, Freeman *et al.* [5] experimentally evidenced two anomalous modes in the energy range of 30–40 and 50–56 meV, which were interpreted following the existence of stripe discommensuration in the checkerboard (CB) matrix. Similar features of the spin wave dispersion have also been observed in $Ln_{2-x}Sr_xNiO_4$ (Ln = La, Nd) with hole doping concentrations in the range $x = 0.45$ to 0.7 [5,16]. Carlson *et al.* [17] suggested the high energy modes, as observed by Freeman *et al.* [5], are due to a twofold direct, instead of a fourfold super-super exchange interactions within the site centered spin stripes. But none of these calculations were carried out taking the discommensuration spin stripe (DCSS) model in the incommensurate spin stripe phases. Furthermore, it is of utmost importance to understand whether such anomalous modes are universal and would apply more generally in isostructural nickelates for similar doping range.

In this Letter we present the magnetic excitations of half-doped $Pr_{3/2}Sr_{1/2}NiO_4$ using inelastic neutron scattering (INS) measurements up to energy transfers of 64 meV and interpret the results taking into account the DCSS model in the LSW calculation.

INS measurements were performed on the thermal triple-axis spectrometer PUMA at the neutron research reactor FRM II in Garching, Germany. Data were collected on a $5 \times 5 \times 4$ mm^3 single crystal of $Pr_{3/2}Sr_{1/2}NiO_4$, grown by the traveling solvent floating zone method [18], with a fixed final energy $E_f = 14.68$ meV of neutrons. The incident and final energies were selected by (002) Bragg reflection of pyrolytic graphite (PG) crystals. A PG filter was used to suppress the higher order harmonics from the scattered neutron beam. The crystal was oriented to measure the spin dynamics in the $(hk0)$-scattering plane. Measurements were performed using a focused monochromator and analyzer configuration of the spectrometer with open collimation. We interpret the results in the pseudotetragonal $F4/mmm$ unit cell with lattice parameters $a = b \sim 5.4$ and $c \sim 12.50$ Å.

For the present case of the DCSS with magnetic incommensurability $\epsilon = 0.4$, Figs. 1(a) and 1(b) illustrate the arrangements of holes and spins in real space, along with specified in- and out-of-plane magnetic exchange interactions in between Ni^{2+} spins. Charge and spin order reflections, indicated in Fig. 2(a) appear by following the

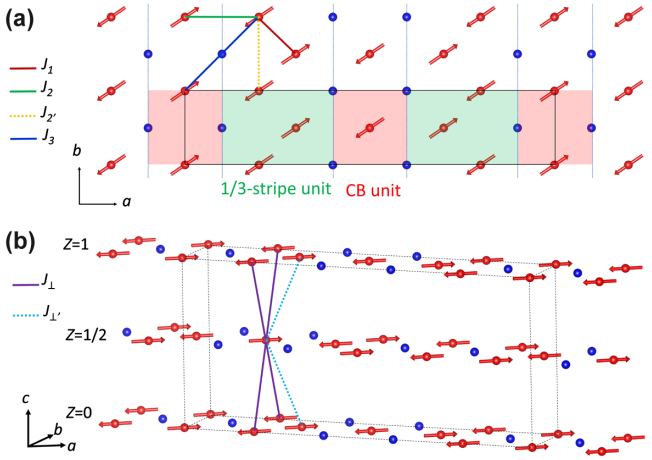

FIG. 1. (a) Schematic representation of the site-centered DCSS unit in NiO_2 plane for a single twin domain of $Pr_{3/2}Sr_{1/2}NiO_4$ consisting of alternating one $1/3$-stripe unit of width $a \times 3/2$ (green shaded box) and one CB unit of width a (red shaded box). The DCSS unit repeats along the a axis of the $F4/mmm$ unit cell. Holes on Ni^{3+} ions (blue spheres) segregate as stripes (dotted blue lines) running diagonal to the $Ni-O-Ni$ bond. Oxygen atoms are omitted for clarity. Spin on the AFM coupled Ni^{2+} ions (red sphere) are indicated by red arrows. The rectangular box in black represents the corresponding magnetic unit cell of length $5 \times a$. Exchange interactions are indicated with different colors. J_2' is identical within both CB and $1/3$ stripe. (b) 3D representation of the DCSS unit cell with the 1st nearest out-of-plane AFM interaction $J_\perp$ and negligible FM interaction $J_{\perp'}$.

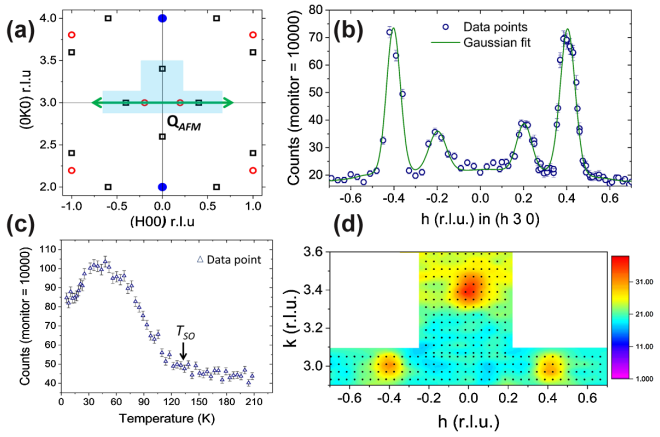

FIG. 2. (a) Diagram of $(hk0)$ plane indicating charge (red circles) and spin (black squares) superlattice reflections for the incommensurability $\epsilon = 0.4$. Blue solid circles represent the nuclear reflections of the parent unit cell. (b) Elastic scan through 030)), marked as a green arrow in (a), indicating two spin order peaks at $(\pm 0.4, 3, 0)$ and two charge order peaks at $(\pm 0.2, 3, 0)$. (c) T-dependent magnetic intensity of the spin peak at (0.4,3,0). (d) Inelastic map of the $(hk0)$ plane at 3 meV in the shaded region in (a). Black dots represent the measurement points.

wave vectors $\mathbf{q}_{\mathrm{CO}} = (\pm 2\epsilon, 0, 1)$ and $\mathbf{q}_{\mathrm{SO}} = (1 \pm \epsilon, 0, 0)$, respectively. Extinction rules for charge and spin order reflections can be found elsewhere Refs. [3,15,19]. The coordinates are given in reciprocal lattice unit $(2\pi/a, 2\pi/b, 2\pi/c)$.

The elastic scan through the Néel antiferromagnetic (AFM) zone center $\mathbf{Q}_{\mathrm{AFM}} = (030)$ in Fig. 2(a) clearly shows the spin and charge order peaks at $(\pm 0.4, 3, 0)$ and $(\pm 0.2, 3, 0)$, respectively, in Fig. 2(b). These peaks imply both charge and spin stripes are running diagonal to the $Ni-O-Ni$ bond. Similarly there are two other satellites at (0,3.4,0) and (0,2.6,0), coming from the twin domain rotated by 90° around the c axis. It is noticeable that the stripe incommensurability $\epsilon = 0.4$ deviates from nominal hole doping concentration $n_h = 0.5$. The linear relationship between incommensurability and hole doping concentration does not hold in nickelates at doping concentrations different from $n_h = \epsilon = 0.333$ for $1/3$ stripes [13]. In our present study the observed periodicity of the spin stripe unit (see Fig. 1), can be explained by the site-centered DCSS model. A mixture of one $1/3$ stripe and one CB unit yields the observed incommensurability $\epsilon = 2/5 = 0.4$ following the model initially proposed by Tranquada *et al.* [15] and later by Yoshizawa *et al.* [13]. The in-plane correlation length calculated from the FWHM of the spin order peak is about $\xi_{\mathrm{SO}} = 27$ Å, which is similar to the length of the DCSS supercell $(5 \times a)$.

Following the T-dependent intensity of the magnetic peak at (0.4,3,0), shown in Fig. 2(c), we find the onset of the spin ordering temperature $T_{\mathrm{SO}} \approx 128$ K, which is in good agreement with magnetic susceptibility measurements (not shown). The observed T_{SO} in our case is also consistent with the well-studied $T - \epsilon$-phase diagram [13,14]. Figure 2(d) represents an inelastic map at 3 meV, reconstructed from several line scans along h in the interval of $\Delta k = 0.025$ r.l.u. Three out of four magnetic peaks are accessible in this scan range. It is clearly noticeable that the magnetic peaks are broadened around $\mathbf{q}_m = (\pm\epsilon, 3, 0)$ and $(0, 3 + \epsilon, 0)$, where $\epsilon = 0.4 \pm 0.05$, without appearing in a ringlike shape indicating their high dispersive nature in the low-energy range as also observed in the case of $La_{2-x}Sr_xNiO_4$ [20].

Figure 3(a) summarizes a series of constant energy scans along h through the magnetic zone centers at $\mathbf{q}_m = (\pm 0.4, 3, 0)$. The spin-wave dispersion was determined by fitting each of the constant-E scans at their corresponding magnetic zone centers with Gaussian profiles and a linear background. Henceforth, in the dispersion, we refer the branches of the spin-wave-like conical modes from $\mathbf{q}_m$, which are approaching towards $\mathbf{Q}_{\mathrm{AFM}}$ as "inner" branches and those are going away from $\mathbf{Q}_{\mathrm{AFM}}$ as "outer" branches. In the 1 meV scan, two weak peaks close to $(\pm 0.2, 3, 0)$ correspond to the dynamics of charge stripes and completely disappear already at 2 meV. Up to 15 meV, the magnetic peaks corresponding to the four branches (two inner and two outer) cannot be resolved completely due to

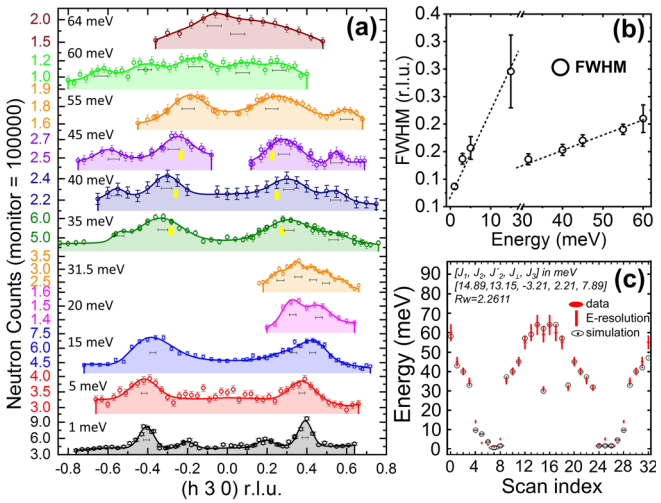

FIG. 3. (a) Constant-E scans through $\mathbf{Q}_{\mathrm{AFM}}$ along h in the range from 1 to 64 meV. Horizontal bars represent the instrumental Q resolution. (b) FWHM of the Gaussian fitted peaks as a function of energy transfer showing the different region of broadening. (c) Refinement results of exchange interactions obtained from the spin wave dispersion fit.

insufficient instrumental resolution to separate the steep spin dispersion with in-plane spin wave velocity of 360 meVÅ in the lower energy regime. For all the scans above 15 meV, where the branches are separated by $\Delta h \geq 0.105$ r.l.u., all four peaks can be resolved. At the maximum energy of the conical modes ~64 meV, two inner branches start to overlap at the $\mathbf{Q}_{\mathrm{AFM}}$, and appears as a broad peak in the scan [Fig. 3(a), top]. However, with closer inspection, it can be clearly seen that the peaks in the energy range 35–45 meV do not appear as expected in the inner branches of the conical modes [marked in the yellow bar in Fig. 3(a)], rather shifted outward symmetrically from $\mathbf{Q}_{\mathrm{AFM}}$ as noticeable in Fig. 4(a). This feature will be elaborated in detail in the following section. Furthermore, the evolution of FWHM of the inelastic magnetic peaks corresponding to the inner branch from $(-0.4, 3, 0)$ for different constant energy scans is given in Fig. 3(b). In the low energy high dispersive region up to 15 meV, we have observed a steep linear increase of FWHM whereas in the high energy region from 20 to 60 meV it is quite flat. The error in measuring the FWHM at 15 meV is larger due to the improper fit of two unresolved peaks. Nevertheless the overall feature of broadening somewhat replicates the combined effect of the broadening in 1/3 stripe and that of the robust CB as reported in Fig. 4(c) of Ref. [16].

To validate and explain the observed characteristic of the measured spin excitation spectra, we have calculated spin wave dispersion based on the LSW theory using the generalized Heisenberg spin-only Hamiltonian given as

$$H = \sum_{i,j} J_{ij} \vec{S}_i \cdot \vec{S}_j, \tag{1}$$

TABLE I. Comparison of all exchange interactions (meV) and coupling constants considered in the present study of $Pr_{2-x}Sr_xNiO_4$ (PSNO) in DCSS model with the other ideal CB and stripe phases of $La_{2-x}Sr_xNiO_4$ (LSNO) from Refs. [4,5,23].

	DCSS (PSNO) (per spin)	Stripe (LSNO [4]) (per spin)	CB (LSNO [5]) (per spin)	CB (LSNO [23]) (per bond)
J_1	14.89 ± 0.29	15 ± 1.5		
J_2	13.15 ± 0.72	$2J_3$		
J_2'	-3.21 ± 0.47			$-0.5J_3$
$J_\perp$	2.21 ± 0.29			
J_3	7.89 ± 0.80	7.5 ± 1.5	5.8 ± 0.5	J_3
$\lambda_{\mathrm{stripe}}$	0.52	0.5		
λ_{CB}	0.6			0.5
λ_{DCSS}	0.88			

where the indices i and j run over all the lattice sites of magnetic atoms and J_{ij} represents all possible exchange interactions acting on Ni^{2+} spins. We have considered the DCSS unit cell shown in Fig. 1(a) for our spin wave calculation with a fair assumption of local spin arrangements to be collinear in the NiO_2 plane like other homologous compounds [4,13,15,21]. Only isotropic Heisenberg exchange interactions in between the $Ni^{2+}(S = 1)$ spins have been considered without any contribution from the $Ni^{3+}(S = 1/2)$ spins. The corresponding Hamiltonian for the site-centered DCSS model as presented in Figs. 1(a), 1(b) was diagonalized using the SpinW code [22]. To determine the strength of the different exchange interactions, we have fitted the experimentally obtained inelastic magnetic wave vectors of the inner and outer branches [see Fig. 3(a)] from total thirteen constant energy scans [2 and 3 meV scans are included but not shown in Fig. 3(a)] using a linear least squares method integrated in the SpinW code and the fit result is shown in Fig. 3(c).

The refined exchange interactions are summarized in Table I along with the characteristic coupling constants defined as $\lambda_{\mathrm{stripe}} = J_3/J_1$, $\lambda_{\mathrm{CB}} = J_3/J_2$ and $\lambda_{\mathrm{DCSS}} = J_2/J_1$ for the ideal 1/3 stripe, CB, and the present DCSS model, respectively. As can be seen from the comparison with other studies on $La_{2-x}Sr_xNiO_4$ [4,5,23], the exchange interactions in our case have very similar strengths and even comparable characteristic coupling constants, which suggests that the magnetic interactions of Ni^{2+} spins in $Pr_{2-x}Sr_xNiO_4$ does not differ enormously from that of $La_{2-x}Sr_xNiO_4$. In the present DCSS model, $\lambda_{\mathrm{DCSS}} \sim 0.88$ is quite similar to the obtained values from theoretical [24] and experimental [2,25] works, suggesting that exchange coupling between Ni^{2+} spins across the charge stripe domain walls is not smaller than the coupling between intrastripe Ni^{2+} spins.

As mentioned earlier, to understand the symmetrical outward shift of the peaks in the range 35–45 meV, we refer

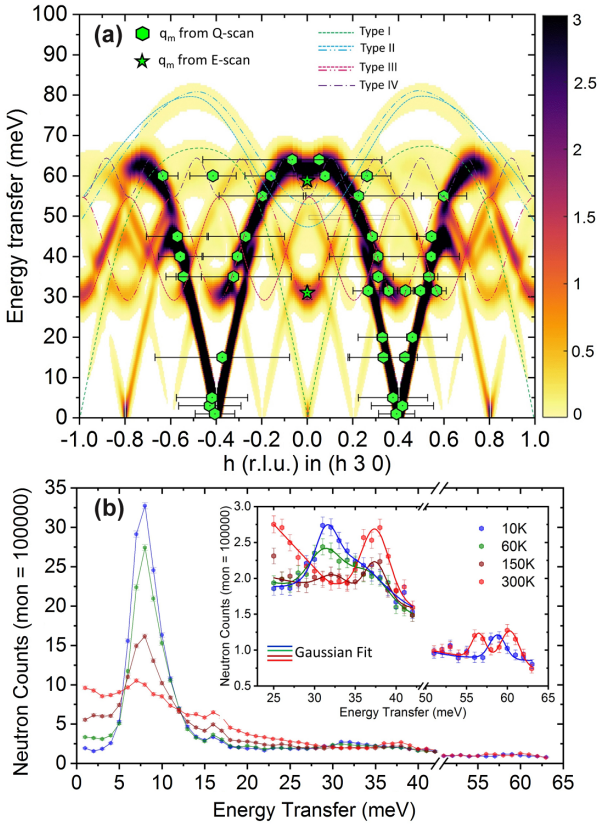

FIG. 4. (a) Intensity convoluted spin wave dispersion in the $(hk0)$ plane overplotted with the measured wave vectors as indicated by green filled hexagons and stars obtained from constant-E and Q scans, respectively. Horizontal and vertical bars in black indicate the FWHMs of the peaks. Dashed lines in different colors represent different type of modes. (b) T dependence of constant-Q scans performed at (0 3 0). Inset shows temperature variation of the magnon and phonon intensities at the region of our interest.

the intensity convoluted spin wave dispersion presented in the color map in Fig. 4(a), which was calculated using the refined exchange interactions. Owing to the known 2D nature of the spin wave dispersion in hole doped nickelates, in the literature so far calculations have been mostly performed neglecting the weak out-of-plane coupling $J_\perp$ in between the AFM coupled Ni^{2+} spins, which has been adequate to describe the commonly expected general features of magnetic excitation spectra but not all of them. However, in our calculation we have considered out-of-plane interaction $J_\perp$, which comes with three different possibilities of stacking the 2D-DCSS NiO_2 plane at $z = 1/2$ along the c axis because the average $F4/mmm$ symmetry of the structure has to be also preserved. The energetically favored configuration as shown Fig. 1(b) gives satisfactory results with zero imaginary eigenvalues of the spin wave modes. For the clarity and simplicity of the explanation, we have named all different energy eigenmodes by type I–IV as labeled in Fig. 4(a). Apparently type-I mode appears with a very low spectral weight dispersing from the $\mathbf{Q}_{\mathrm{AFM}}$ similar to what was found in Yao *et al.* [23] for the ideal CB system, and the type-II mode with a dip at $\mathbf{Q}_{\mathrm{AFM}}$ in the energy range ~47 and 52 meV, has not been reported so far. The anomalous mode observed by Freeman *et al.* [5] may resemble one of these types (I or II). However, we have noticed in our calculation that the energy range for type-II modes depends on the particular number of 1/3-stripe and CB units in the DCSS unit cell and on the strength of the in-plane couplings. The maximum energy (~64 meV) of the magnetic excitations observed in $Pr_{3/2}Sr_{1/2}NiO_4$ lies in between the maximum energy of the magnetic excitation spectra of $La_{2-x}Sr_xNiO_4$ in 1/3 stripe ($E_{max} \sim 90$ meV) and CB ($E_{max} \sim 40$ meV) phases [4,5]. The type-I and type-II modes emerge only in the presence of twin domains and its spectral weight depends on the twin volume fraction.

From Fig. 1(b) it can be seen that the out-of-plane interactions in between the Ni^{2+} spins is somewhat frustrated. However, the FM interactions $(J_{\perp'})$ have been neglected as it creates conical modes with strong spectral weight at $\mathbf{Q}_{\mathrm{AFM}}$ and much weaker spectral weight at $(\pm 0.4, 3, 0)$, which is not consistent with the experimentally obtained dispersion. Therefore, we have considered only the 1st nearest out-of-plane interactions $(J_\perp)$ in between Ni^{2+} spins running diagonally as 1D-AFM chain in the $(b - c)$ plane. This leaves the system with a quasi-3D magnetic ordering. Very importantly, inclusion of out-of-plane interaction $(J_\perp)$ gives rise to two other sinusoidal modes (type III) having π-phase shift to each other, and with different spectral weight in the energy range from ~28 to 54 meV. One of these type-III sinusoidal modes with a dip at the $\mathbf{Q}_{\mathrm{AFM}}$ overlaps with the inner branches leading to the observed symmetrical outward shift of the magnetic peaks in the energy range 35–45 meV, where the peaks are centered on the corresponding type-III mode with maximum intensity. The instrumental resolution even for the scan at 35 meV (~0.055 r.l.u) was not enough to resolve the splitting (calculated to be $\sim 0.045 \pm 0.005$ r.l.u.) between type III and the inner branches. However, a constant-E scan performed at 31.5 meV, where the splitting between the above mentioned modes are expected to be larger, reveals four peaks corresponding to conical modes [(0.273, 3, 0) and (0.498, 3, 0)] and type-III modes [(0.357,3,0) and (0.429, 3, 0)], respectively, as shown in Fig. 3(a).

For an unambiguous determination of the type-III mode and to confirm its magnetic origin we have performed T-dependent constant-Q scans at (0 3 0). Figure 4(b) clearly shows upon heating from 10 K the intensity of the type-III mode (~31 meV) starts to decrease and persist up to 150 K, whereas the phonon (~37 meV) intensity increases with temperature. The intensity at ~8 meV increases at low temperature due to the emergence of strong crystalline electric field (CEF) excitation as found similarly in $Nd_{2-x}Sr_xNiO_4$ [16]. Nevertheless, from the

calculation we have observed a very weak mode (type-IV) which may come from the increased number of magnetic atoms in the DCSS unit cell. Overall, calculated spin wave dispersion accounting for the DCSS model of $Pr_{3/2}Sr_{1/2}NiO_4$ provides an excellent description of the measured magnetic excitation spectra.

In summary, we have measured spin excitations in half-doped $Pr_{3/2}Sr_{1/2}NiO_4$ up to 64 meV and the results are in good accordance with the LSW calculation performed on the discommensuration spin stripe model. Consideration of AFM out-of-plane interaction ($J_\perp$) together with in-plane interactions were essential to account for the symmetrical outward shift of the magnetic peaks form the Néel AFM zone center in the mid energy range of the spectra. Calculated characteristic coupling constant $\lambda_{\mathrm{DCSS}} \approx \lambda_{\mathrm{stripe}} + \lambda_{\mathrm{CB}}$ from the refined exchange interactions illustrate that the real arrangement of holes on Ni^{3+} sites and Ni^{2+} is indeed as expected from the DCSS model. Therefore, our study suggests that such a detailed DCSS model with careful consideration of the out-of-plane coupling between AFM coupled Ni^{2+} spins ($S = 1$) is necessary to uncover many unexplained features of spin wave dispersion quantitatively in these strongly correlated nickelates, cobaltates, and particularly in the doping range in which magnetic ordering is incommensurate.

We would like to greatly acknowledge the support of M. Ceretti for providing us with good quality single crystal. We thank M. Opel for helping with the SQUID magnetometry measurements, J. T. Park for giving important tips during INS measurements at PUMA, and S. Ward for helpful discussion regarding the SpinW code. A. M. would like to greatly acknowledge the support of G. Eckold for giving the opportunity to use internal neutron beamtime at the instrument PUMA at FRM II operated by Georg-August-Universität Göttingen in cooperation with Technische Universität München.

*Corresponding author.
avishek.maity@frm2.tum.de
†Corresponding author.
rajesh.dutta@frm2.tum.de

[1] J. M. Tranquada, P. Wochner, and D. J. Buttrey, Phys. Rev. Lett. **79**, 2133 (1997).
[2] P. Bourges, Y. Sidis, M. Braden, K. Nakajima, and J. M. Tranquada, Phys. Rev. Lett. **90**, 147202 (2003).
[3] S. Anissimova, D. Parshall, G. D. Gu, K. Marty, M. D. Lumsden, S. Chi, J. A. Fernandez-Baca, D. L. Abernathy, D. Lamago, J. M. Tranquada, and D. Reznik, Nat. Commun. **5**, 3467 (2014).
[4] A. T. Boothroyd, D. Prabhakaran, P. G. Freeman, S. J. S. Lister, M. Enderle, A. Hiess, and J. Kulda, Phys. Rev. B **67**, 100407(R) (2003).
[5] P. G. Freeman, A. T. Boothroyd, D. Prabhakaran, C. D. Frost, M. Enderle, and A. Hiess, Phys. Rev. B **71**, 174412 (2005).
[6] P. G. Freeman, S. R. Giblin, K. Hradil, R. A. Mole, P. Cermak, and D. Prabhakaran, Phys. Rev. B **95**, 064403 (2017).
[7] A. T. Boothroyd, P. G. Freeman, D. Prabhakaran, A. Hiess, M. Enderle, J. Kulda, and F. Altorfer, Phys. Rev. Lett. **91**, 257201 (2003).
[8] J. M. Tranquada, B. J. Sternlieb, J. D. Axe, Y. Nakamura, and S. Uchida, Nature (London) **375**, 561 (1995).
[9] B. O. Wells, Y. S. Lee, M. A. Kastner, R. J. Christianson, R. J. Birgeneau, K. Yamada, Y. Endoh, and G. Shirane, Science **277**, 1067 (1997).
[10] N. B. Christensen, D. F. McMorrow, H. M. Rønnow, B. Lake, S. M. Hayden, G. Aeppli, T. G. Perring, M. Mangkorntong, M. Nohara, and H. Tagaki, Phys. Rev. Lett. **93**, 147002 (2004).
[11] B. Vignolle, S. M. Hayden, D. F. McMorrow, H. M. Rønnow, B. Lake, C. D. Frost, and T. G. Perring, Nat. Phys. **3**, 163 (2007).
[12] M. Matsuda, M. Fujita, S. Wakimoto, J. A. Fernandez-Baca, J. M. Tranquada, and K. Yamada, Phys. Rev. Lett. **101**, 197001 (2008).
[13] H. Yoshizawa, T. Kakeshita, R. Kajimoto, T. Tanabe, T. Katsufuji, and Y. Tokura, Phys. Rev. B **61**, R854 (2000).
[14] R. Kajimoto, K. Ishizaka, H. Yoshizawa, and Y. Tokura, Phys. Rev. B **67**, 014511 (2003).
[15] J. M. Tranquada, D. J. Buttrey, V. Sachan, and J. E. Lorenzo, Phys. Rev. Lett. **73**, 1003 (1994).
[16] Y. Ikeda, S. Suzuki, T. Nakabayashi, H. Yoshizawa, T. Yokoo, and S. Itoh, J. Phys. Soc. Jpn. **85**, 023701 (2016).
[17] E. W. Carlson, D. X. Yao, and D. K. Campbell, Phys. Rev. B **70**, 064505 (2004).
[18] O. Wahyudi, M. Ceretti, I. Weill, A. Cousson, F. Weill, M. Meven, M. Guerre, A. Villesuzanne, J.-M. Bassat, and W. Paulus, CrystEngComm **17**, 6278 (2015).
[19] R. Zhong, B. L. Winn, G. Gu, D. Reznik, and J. M. Tranquada, Phys. Rev. Lett. **118**, 177601 (2017).
[20] H. Woo, A. T. Boothroyd, K. Nakajima, T. G. Perring, C. D. Frost, P. G. Freeman, D. Prabhakaran, K. Yamada, and J. M. Tranquada, Phys. Rev. B **72**, 064437 (2005).
[21] A. M. Merritt, D. Reznik, V. O. Garlea, G. D. Gu, and J. M. Tranquada, Phys. Rev. B **100**, 195122 (2019).
[22] S. Toth and B. Lake, J. Phys. Condens. Matter **27**, 166002 (2015).
[23] D. X. Yao and E. W. Carlson, Phys. Rev. B **75**, 012414 (2007).
[24] F. Krüger and S. Scheidl, Phys. Rev. B **67**, 134512 (2003).
[25] R. Klingeler, B. Büchner, S.-W. Cheong, and M. Hücker, Phys. Rev. B **72**, 104424 (2005).